JMEPEG (2009) 18:886–892
DOI: 10.1007/s11665-008-9306-5

1059-9495/$19.00

# Advanced Production Process and Properties of Die Cast Magnesium Composites Based on AZ91D and SiC

*German Gertsberg, Eli Aghion, Ali Arslan Kaya, and Dan Eliezer*

*(Submitted November 14, 2007; in revised form August 6, 2008)*

**The driving force behind the efforts to develop magnesium metal matrix composites (MMC) via high-pressure die casting is the requirements for advanced applications under severe operational conditions in terms of stress, temperature, and corrosion resistance. Therefore this study aims to explore the mechanical properties of die cast Mg-MMC in terms of hardness and strength, as well as its corrosion resistance. AZ91D was chosen as the most commonly used magnesium alloy. The choice as the reinforcement agent that has to be an economical and non-reactive addition was silicon carbide particles ($SiC_P$) with an average particle size of 10 μm. The challenge was production of high quality, homogeneous material with good mechanical properties and acceptable corrosion resistance. The results revealed the advantages of a die cast Mg-MMC as a new attractive alternative for advanced structural applications that can be used for mass production.**

**Keywords** die casting, magnesium, metal matrix composites

## 1. Introduction

In order to obtain high quality, sound components of die cast Mg-MMC, the main challenge is the optimization of die casting process to achieve uniformity and reproducibility given the condition that the matrix alloy and the reinforcement are suitable (Ref 1-4). Only then could a new attractive material presenting superior mechanical properties be expected.

The desired mechanical properties in terms of wear, tensile, and fatigue under high stresses and temperatures need also be coupled with improved physical properties, such as thermal conductivity, thermal expansion, and dimensional stability. In this regard, the Mg-MMC alloys can be ''tailored'' according to the application requirements with a critically established amount of reinforcement particles (Ref 5). Currently, only squeeze casting or infiltration methods are being used for the production of MMC components. These previous investigations have shown that the undesirable reactivity between SiC phase and AZ91 alloy matrix was reduced as compared to the other alloys of magnesium (Ref 6-8).

This work attempts to assess the challenges involved in the production of Mg-MMC materials via HPDC and process optimization, and evaluates the effects of the reinforcement particles on the properties and performance of this new material.

**German Gertsberg**, Magnesium Research Institute, P.O. Box 1195, Beer-Sheva 84111, Israel; **Eli Aghion** and **Dan Eliezer**, Department of Materials Engineering, Ben-Gurion University of the Negev, P.O. Box 653, Beer-Sheva 84105, Israel; and **Ali Arslan Kaya**, Department of Metallurgy and Materials Science Engineering, Mugla University, Mugla 48170, Turkey. Contact e-mail: germang@dsmag.co.il.

## 2. Experimental Procedures

The production procedure of magnesium metal matrix composite (Mg-MMC) by die casting consists of two main stages, namely incorporation of reinforcement particles into molten alloy AZ91D and die casting of a part using this mixture.

### 2.1 Materials

The most common die casting Mg alloy was selected as matrix material.

Table 1-3 presents the chemical compositions of ingot and die casting forms, physical and mechanical properties of AZ91D.

The matrix alloy was reinforced by SiC particles, which were 10 μm in average size. The chemical composition and properties of the SiC used in the present investigation are shown in Table 4 and 5, respectively.

Two different mixing ratios, 5 and 10 wt.%, were used for composite production. This upper limit of 10% was set by the high-pressure die castability of the mixtures. Higher quantities of $SiC_P$ addition, e.g. 15 wt.%, proved extremely difficult due to sticking problem in the die.

### 2.2 Material Preparation

The aim of the optimization procedure is to minimize chemical reactions between the molten metal and the particles during processing, to produce composite materials with homogeneous distribution of reinforcement particles and a minimum level of microstructural defects.

Extensive trials showed that a number of parameters were very important for the optimization of the process. The molten alloy temperature before the introduction of $SiC_P$ and the casting temperature are two of the important parameters to be controlled carefully. Furthermore, the pattern of introduction of $SiC_P$ and stirring parameters themselves were critically important to achieve good quality composite structures.

**Table 1 Chemical compositions of AZ91D (in wt.%)**

| State | Al | Mn | Zn | $Si_{Max}$ | $Cu_{Max}$ | $Ni_{Max}$ | $Fe_{Max}$ |
|---|---|---|---|---|---|---|---|
| Ingot | 8.5-9.5 | 0.17-0.4 | 0.45-0.9 | 0.05 | 0.025 | 0.001 | 0.004 |
| Die cast | 8.3-9.7 | 0.15-0.5 | 0.35-1.0 | 0.10 | 0.030 | 0.002 | 0.005 |

**Table 2 Physical properties of AZ91D**

| Density, g/cm$^3$ | Solidus temperature, °C | Liquidus temperature, °C | Casting temperature, °C | Latent heat, kJ/kg | Specific heat, kJ/kg K | Thermal conductivity, W/K m |
|---|---|---|---|---|---|---|
| 1.81 | 437 | 598 | 660-680 | 370 | 1.02 | 51.0 |

**Table 3 Mechanical properties of AZ91D**

| TYS, MPa | UTS, MPa | *E*, % | Impact, J/cm$^2$ | Young's modulus, GPa | Hardness Brinell |
|---|---|---|---|---|---|
| 160 | 240 | 5 | 4 | 45 | 70 |

**Table 4 Chemical compositions of SiC**

| Components | SiC | $SiO_2$ | C | Si | $Al_2O_3$ | $Fe_2O_3$ |
|---|---|---|---|---|---|---|
| Wt.% | 98.0 | 0.75 | 0.40 | 0.60 | 0.20 | 0.005 |

**Table 5 Mechanical and physical properties of SiC**

| Density, g/cm$^3$ | Bending strength, MPa | Compressive strength, MPa | Young's modulus, GPa | Hardness Vickers, GPa | Thermal expansion, $10^{-6}$ K$^{-1}$ | Thermal conductivity, W/K m |
|---|---|---|---|---|---|---|
| 3.2 | 400 | 2200 | 400 | 24.5 | 3.5 | 100 |

About 16 kg AZ91D ingots were re-melted in steel crucible up to 640 °C under the protection of a gas mixture of 99.5% $CO_2$ + 0.5% $SF_6$. Reinforcement particles ($SiC_P$) were pre-heated to 700 °C under argon atmosphere. The following three methods were tried to introduce $SiC_P$ particles into the molten alloy:

1. Entry of a package of particles wrapped in aluminum foil into the melt during stirring.
2. Entry of the lose particles through the free surface of the molten alloy during stirring.
3. Bottom entry of the lose particles during stirring of the melt through a spill immersed in the melt.

The best results were obtained using the third method. The rate of particle feeding was about 150 g/min that was determined by the diameter of the spill. This rate also seemed to allow a good mixing and a homogeneous dispersion of the particles in the molten metal. A schematic drawing of the experimental setup for this method is given in Fig. 1.

Following the introduction of the particles while stirring the melt, the stirring was stopped and the melt was held for 2 h in order to achieve good wetting of the particles by the molten metal (Ref 8). Using holding time shorter than 2 h resulted in undesirable increased porosity. Following this the stirring was resumed for 15 min. Stirring was done at a frequency of 10 Hz, which is sufficient for a good intensive stirring (Ref 9). The effect of insufficient stirring of the melt is presented in Fig. 2. Figure 2(a) shows the microstructure achieved after 5 min stirring and Fig. 2(b) presents the case where the stirrer rotation velocity is kept low. The result of optimized stirring conditions is illustrated in Fig. 2(c), i.e. the stirrer rotation velocity 10 Hz

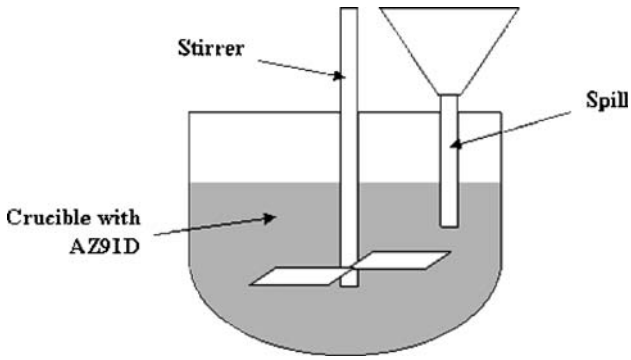


**Fig. 1** Experimental crucible equipment

and stirring time 15 min. In general, it was evident that inadequate stirring process resulted in an inhomogeneous dispersion of the SiC particles in the alloy matrix and consequently non-homogeneous properties of the MMC material system.

The flow chart of the optimized production procedure is given in Fig. 3.

### 2.3 Casting Procedure

Tensile, creep, fatigue, immersion corrosion, and impact strength specimens were die cast using MRI's (Magnesium Research Institute) IDRA OL-320 cold chamber die casting machine with a locking force of 345 ton, and a special die (Fig. 4) containing cavities of required dimensions for each of the specimen types. The gates area is 0.57 cm$^2$.

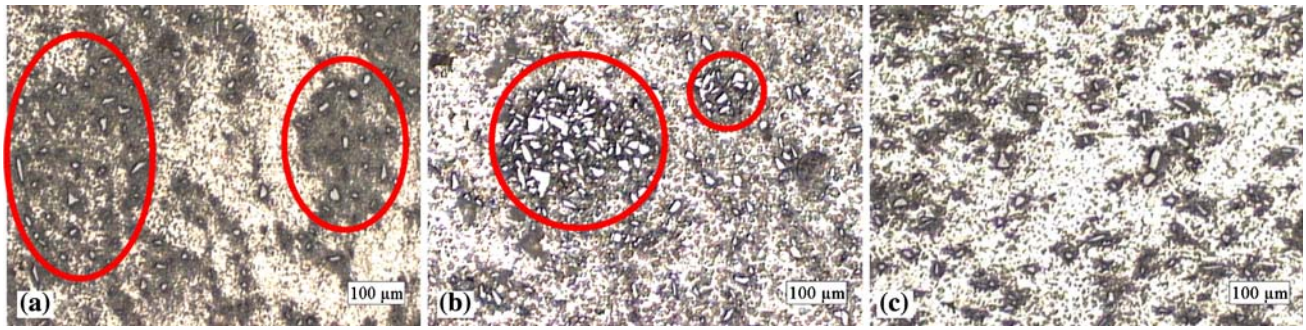


**Fig. 2** Influence of stirring process on microstructure: (a) short stirring period, (b) low stirring velocity, and (c) optimized stirring conditions

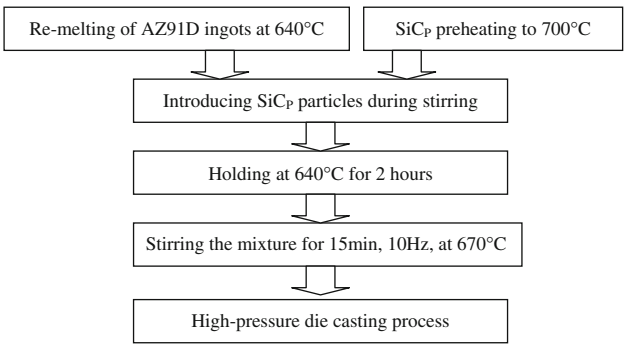


**Fig. 3** Flow chart showing the optimized processing sequence and conditions

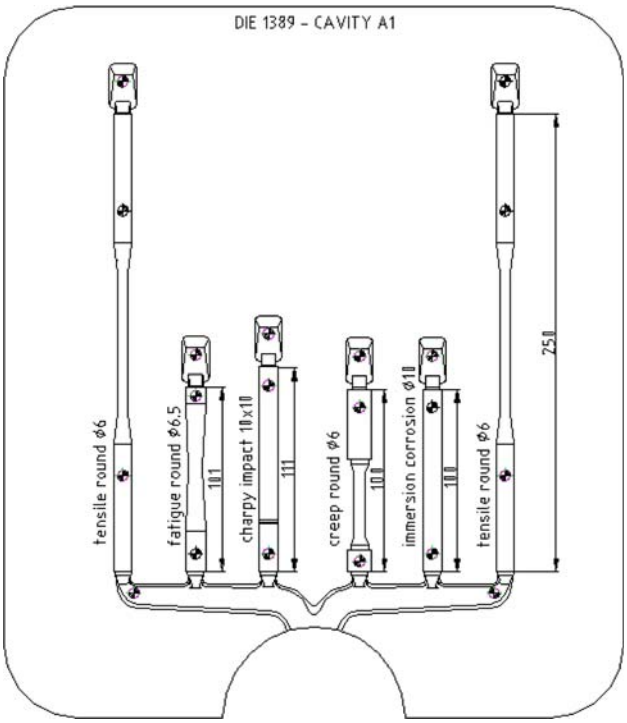


**Fig. 4** Schematic drawing of the die containing various specimen cavities

Shot-sleeve filling ratio was about 30% and conducted at a temperature of 200 °C. Sticking phenomena was evaluated in the gates area (the smallest transverse cross section through which the metal is introducing into the die cavities), considering the variation of viscosity as a result higher gate velocities (Ref 10, 11). Thus the die-sticking problem was eliminated by reducing the die surface temperature from the originally used temperature of 200 °C for AZ91D, to 150 °C, and by employing richer lubrication of the dies (Ref 12). As it was described above, the MMC with 15 wt.% $SiC_P$ was regarded as non-castable in terms of sticking near the gates area, for which our optimized conditions were not effective. In order to avoid sticking, gates areas would have to be increased, which would then result in a decrease in the gate velocity and elimination of defects.

### 2.4 Microstructural Examination

The microstructure of the specimens was examined using an SEM (JOEL JSM-35C with a resolution of 60 Å, operated at 25 kV), and a light microscope (Nikon Metallurgical Microscope OPTIPHOT). The specimens for microscopy were prepared by standard wet grinding using SiC abrasive papers and diamond paste followed by etching with oxalic acid. The microstructure images were taken from the same areas of the castings to have comparable cases. Grains size analysis was based on line intercept method, which is a standard procedure in quantitative microscopy. In this method the number of grains along each line is counted and the average grain diameter is calculated (according to the line length, image scale and magnification). The following equation presents the grain size measurement technique.

$$\text{Grain Size } [\mu] = \frac{\text{Dimensional Length } [\text{m}]}{\text{Magnification}} \times \left(\frac{1}{\text{Nuclei Counted}}\right)$$

### 2.5 Tensile Tests

The tensile specimens with the gage length of 750 mm and diameter of 6 mm were prepared in accordance with the ASTM B557M standard. Mechanical properties were tested using an Instron 8500 series tensile testing machine with a crosshead speed of 0.2 mm/min up to tensile yield strength (TYS) and 0.5 mm/min for the remaining of the tests up to rupture.

### 2.6 Hardness

Macro hardness of Mg and Mg/SiC samples was determined using the Rockwell F scale. Rockwell hardness measurements were made using a 1/16 in. diameter steel ball indenter with a 60 kgf test load, in accordance with ASTM E18-92 standard. The measurements were performed on rectangular specimen having the dimensions of $10 \times 10 \times 100$ mm.

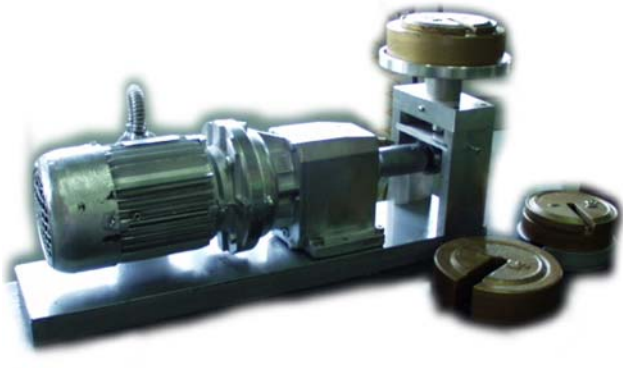

**Fig. 5** Wear resistance testing machine designed at MRI

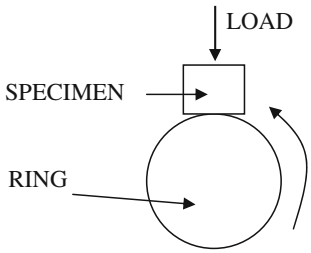


**Fig. 6** Schematic diagram showing block-on-ring wear test ring

### 2.7 Density Measurements

The densities of samples were determined using the Archimedes' principle to quantify the volume fraction of porosity. The density measurements involved the weighing of samples in air and when immersed in distilled water. The densities, derived from the recorded weights, were then compared to the theoretical densities based on the rule of mixtures from which the volume fractions of porosity were calculated. At least ten specimens were taken into consideration to obtain an average density for each material. The specimens were taken from all areas of casting.

### 2.8 Wear Resistance Testing

The wear tests on Mg alloys were conducted on a block-on-ring type wear resistance testing machine, which was developed at MRI. The equipment is shown in Fig. 5.

The test conditions were as follows: sliding speed 300 rpm (about 1.9 m/s), sliding time 60 min (about 2909 m in sliding distance), and loads 5-120 N.

A schematic illustration of the test is given in Fig. 6.

The weight losses were calculated based on the weight of the specimens ($6 \times 6 \times 10$ mm) before and after the wear tests. The wear rate, defined as the weight loss percentage per unit sliding distance, was then plotted against load in order to compare different samples.

### 2.9 Corrosion Immersion Test

Corrosion tests were performed according to ASTM standard B117. This standard requires the use of 5% NaCl test solution at pH 11.5 and a cabinet temperature of 35 °C. Round specimens of 10 mm diameter and 100 mm length were exposed for various lengths of time, namely 24, 48, 72, and 96 h. At the end of each test, the corrosion products were cleaned by immersion in

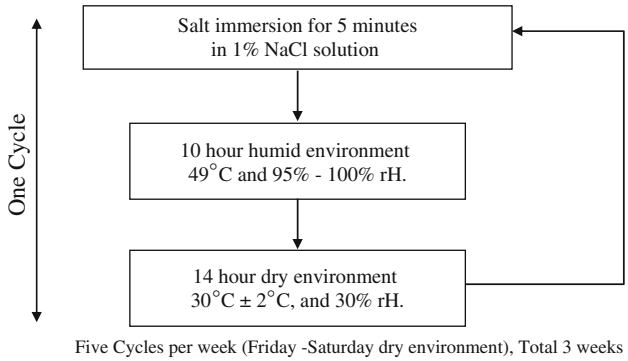


**Fig. 7** Cyclic corrosion test experimental procedure

chromic acid solution (180 g $CrO_3$ per liter solution plus 1% silver nitrate) at 80 °C for about 20 min, and the weight loss is determined after rinsing with hot water and drying in a stream of air. The weight loss is used to determine the average corrosion rate (C.R.) over the test period in mille-inch per year (mpy).

### 2.10 Cyclic Corrosion Test

In order to simulate the behavior of material during service in vehicles, the cyclic procedure employed is shown in Fig. 7.

Specimen's type, cleaning after test, and weight loss determination procedure were all similar to those of the corrosion immersion test.

### 2.11 Electrochemical Testing

Electrochemical polarization experiments were carried out using round specimens which were immersed in a corrosion cell containing of 3.5% NaCl solution with the steady state pH of 10.5 and a polarization scan rate of 1 mV/s.

## 3. Results and Discussion

### 3.1 Microstructure

Figure 8 shows the homogeneous distribution of $SiC_P$ except for a skin layer. The particle distributions can be evaluated for various distances from the surface.

The matrix microstructure of MMC is typical of the HPDC structure with a bimodal grain size distribution (Fig. 9). The average grain size increases as the distance from the surface increases. It can also be noticed that the average grain size of AZ91D matrix decreases with increasing percentage of reinforcement.

The average grain size of the microstructures given in Fig. 8 and 9 was determined by using line intercept method, and the results are given in Fig. 10.

It is evident that the microstructure became finer as the percentage of $SiC_P$ increases. The reinforcement particles probably facilitate the nucleation of new grains during solidification, thus reducing the average grain size. The effect was also observed during MMC fabrications using other casting methods (Ref 5, 9).

A good wetting of reinforcement particles by the matrix is a prerequisite for the success of the MMC to ensure the load transfer across the matrix/particle interface. Figure 11 shows the level of wetting and the resulting good adherence at the SiC particle surfaces.

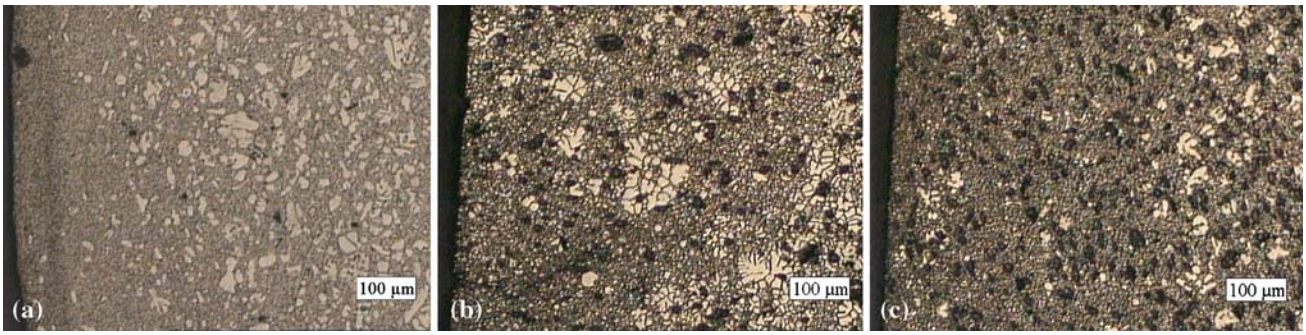


**Fig. 8** The distribution of $SiC_P$ close to the surface of die cast parts: (a) AZ91D, (b) AZ91D + 5 wt.% $SiC_P$, and (c) AZ91D + 10 wt.% $SiC_P$

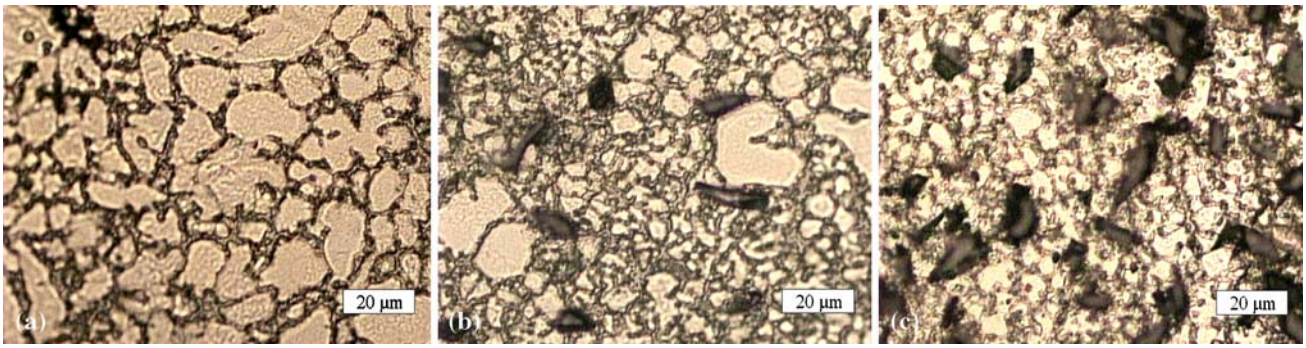


**Fig. 9** The microstructure of die cast material: (a) AZ91D, (b) AZ91D + 5 wt.% $SiC_P$, and (c) AZ91D + 10 wt.% $SiC_P$

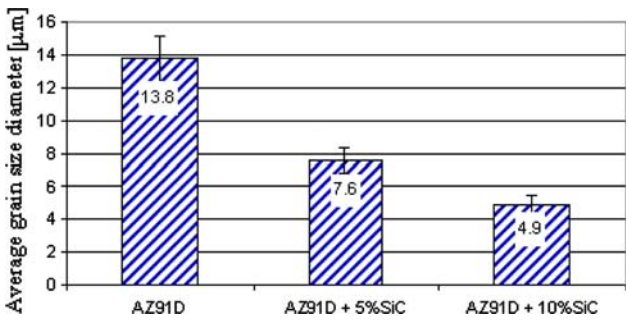


**Fig. 10** The effect of the amount of $SiC_P$ on the average grain size

It can also be observed that primary $\alpha_{Mg}$ grains surrounded by eutectic mixture of $\alpha_{Mg}$ and $\beta$-$Mg_{17}Al_{12}$ and that SiC particles pushed by primary $\alpha_{Mg}$ phase into the last solidification regions, i.e. the grain boundaries. On the other hand, the SiC particles work as a barrier preventing grain growth. This fact explains the decrease in average grain size with increasing of SiC. Very few reinforcement particles can be observed within the $\alpha_{Mg}$ grains. The interface area of the matrix with SiC is also mainly associated with $\beta$-$Mg_{17}Al_{12}$.

The precipitations were probably formed due to the reaction: $SiC + 2\ Mg \rightarrow Mg_2Si + C$ (Ref 7). Although very rarely some $Mg_2Si$ precipitations of round form with average diameters of ~1 µm were also detected close to the SiC particles.

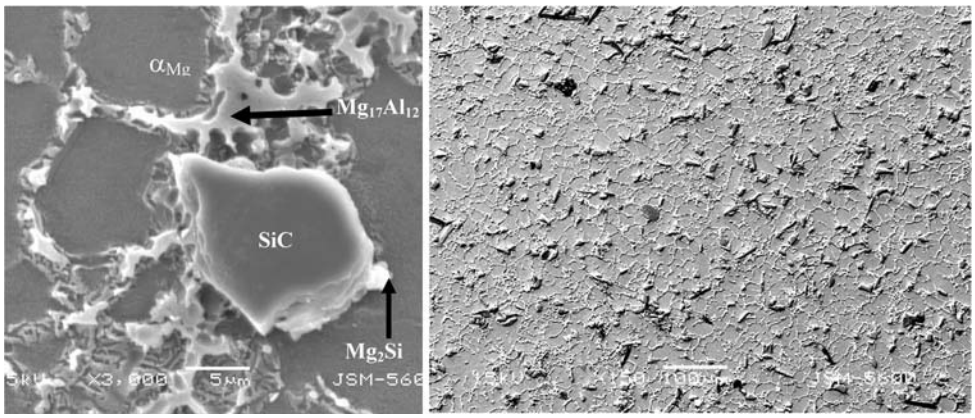


**Fig. 11** SEM micrographs of MMC structures

### 3.2 Density

The measured density values, determined using the Archimedes' principle, were compared with the theoretical values, based on the rule of mixtures, as it was described in Sect. 2, in order to determine the rate of porosity formation. Table 6 shows that addition of SiC particles resulted in an increase in porosity with increasing percentage of particles as compared to the monolithic alloy.

### 3.3 Mechanical Properties

The results of mechanical properties evaluation at room temperature are presented in Table 7. Addition of SiC seems to increase the TYS, while ultimate tensile strength (UTS) and elongation decreased.

TYS did not seem to increase linearly with increasing amount of reinforcement as shown in Fig. 12. SiC addition to the matrix is a process that also led to some defects like porosity, possibly resulting from the mixing and gases trapped in the particle clusters. The positive effect of $SiC_P$ on the TYS appears to be more pronounced when tensile testing was conducted at higher temperatures (up to 175 °C). The Mg-MMC with 10% wt. of $SiC_P$ presented significantly improved TYS properties (up to 50%) at higher temperatures (see Fig. 12).

Hardness levels were also shown to increase with reinforcement.

**Table 6 Density measurements results**

| Material | Volume fraction, % | Density, g/cm$^3$ | Calculated density, g/cm$^3$ | Porosity, % |
|---|---|---|---|---|
| AZ91D | 0 | 1.791 | 1.8 | 0.5 |
| AZ91D + 5 wt.% $SiC_P$ | 2.88 | 1.790 | 1.806 | 0.9 |
| AZ91D + 10 wt.% $SiC_P$ | 5.88 | 1.839 | 1.882 | 2.1 |

**Table 7 Mechanical properties at room temperature**

| Material | UTS, MPa | TYS, MPa | Elongation, % | Hardness, HRF |
|---|---|---|---|---|
| AZ91D | 240 | 160 | 5 | 78 |
| AZ91D + 5 wt.% $SiC_P$ | 217 | 185 | 1 | 82 |
| AZ91D + 10 wt.% $SiC_P$ | 220 | 180 | 1 | 83 |

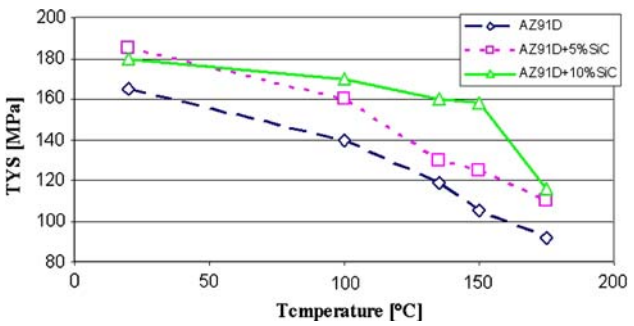


**Fig. 12** The change in the TYS with testing temperature

Table 7 shows that the hardness of MMC is highly dependent on the SiC percentage.

### 3.4 Wear Resistance

The wear rate in terms of weight loss versus load plots for the magnesium systems studied is shown Fig. 13.

The observation of wear surfaces showed that at high loads the removal of material from the surface of composite specimens occurred due to the higher level of porosity in these samples, while the worn surfaces of AZ91 were relatively smoother.

### 3.5 Environmental Behavior

Environmental behavior evaluation tests results, namely corrosion immersion, cyclic test, and potential dynamic, are presented in Fig. 14-16, respectively. It is clearly evident that the corrosion rate increased as the percentage of reinforcement increases. This tendency is true for all general corrosion tests employed in this study.

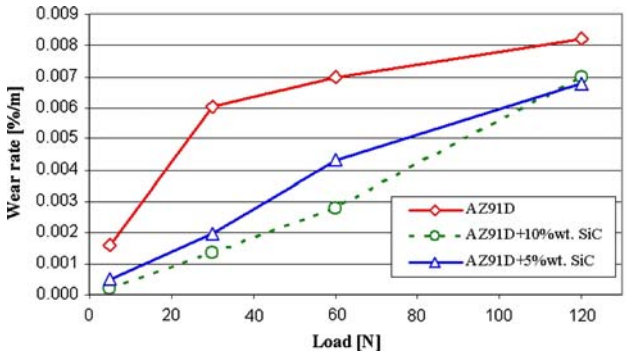


**Fig. 13** Weight wear rate versus load

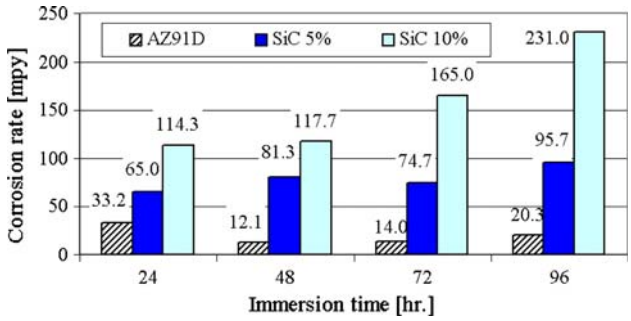


**Fig. 14** Corrosion immersion test results

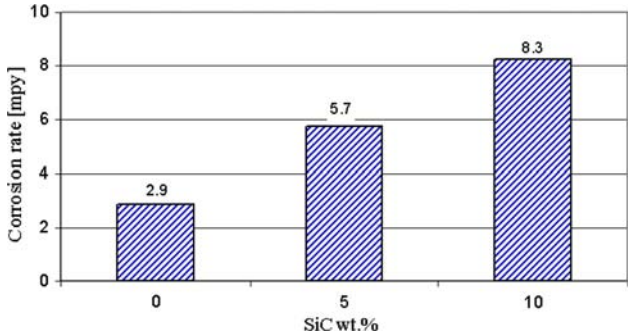


**Fig. 15** Cyclic corrosion test results

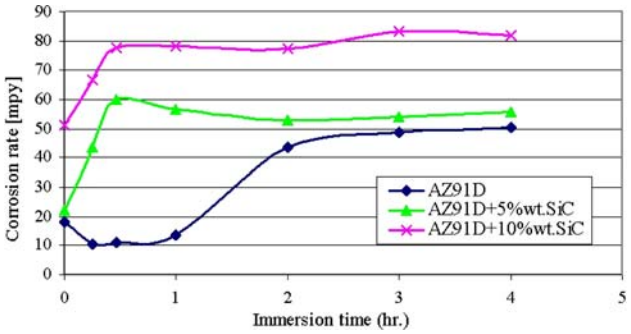


**Fig. 16** Potentiodynamic polarization results in terms of corrosion rate versus immersion time

The degradation in the environmental behavior is mainly attributed to the micro-galvanic effect between the $SiC_P$ particles and the alloy matrix. Additional detrimental effect on the corrosion resistance is caused by the inherent porosity that is enhanced by the presence of SiC particles.

## 4. Conclusions

1. An advanced production procedure for die cast Mg-MMC material system has been developed. The obtained material quality in terms of defects such as porosity may be optimized by using special die design and by modifying the gates structure.
2. The effects of the reinforcement particles on the properties of die cast Mg-MMC were evaluated. Die cast Mg-MMC exhibits superior high-temperature performance as well as improved wear resistant.
3. The influence of the reinforcement particles on the processing characteristics, namely microstructure and porosity, has been evaluated. Microstructure became finer as the quantity of reinforcement particles increased.
4. Increasing the amount of $SiC_P$ particles has a negative effect on the environmental performance of the Mg-MMC material system. This was mainly attributed to the galvanic effect and porosity created by the SiC particles.

## References

1. ASM Metals Handbook, *Die Casting*, 10th ed., ASM, Metals Park, OH, 1995, p 286–295
2. International Magnesium Association, *The Essentials of Magnesium Die Casting*, 1991, p 10
3. International Magnesium Association, *Magnesium Die Castings*, 1992, p 8
4. E. Aghion, B. Bronfin, and D. Eliezer, The Role of the Magnesium Industry in Protecting the Environment, *J. Mater. Process. Technol.*, 2001, **117**, p 381–385
5. M. Jayamathy, S. Seshan, S.V. Kailas, K. Kumar, and T.S. Srivatsan, Influence of Reinforcement on Microstructure and Mechanical Response of a Magnesium Alloy, *Curr. Sci.*, 2004, **87**(9), p 1218–1231
6. E. Aghion, B. Bronfin, N.F. Von Buch, S. Schumann, and H. Friedrich, Newly Developed Magnesium Alloys for Powertrain Applications, *JOM*, 2003, **55**, p 30–33
7. M. Zheng, K. Wu, and C. Yao, Effect of Interfacial Reaction on Mechanical Behavior of SiCw/AZ91 Magnesium Matrix Composites, *Mater. Sci. Eng. A*, 2001, **318**, p 50–56
8. S. Young-Ho, The Simulation of the Viscoplastic Forming Process by the Finite-Element Method, *J. Mater. Process. Technol.*, 1995, **55**, p 370–379
9. J. Hashim, L. Looney, and M.S.J. Hashmi, Metal Matrix Composites: Production by the Stir Casting Method, *J. Mater. Process. Technol.*, 1999, **93**, p 1–7
10. N. Moscovitch, D. Eliezer, and E. Aghion, The Effect of High Pressure Die Casting Process Characteristics on the Properties and Performance of Advanced Mg Alloys, in *Magnesium Technology 2005*, N.R. Neelameggham, H.I. Kaplan and B.R. Powell, Eds., TMS, Warrendale, PA, 2005, p 357–363
11. B. Bronfin, et al., Die Casting Magnesium Alloys for Elevated Temperature Applications, in *Magnesium Technology*, J.N. Hryn, Ed., TMS, Warrendale, PA, 2001, p 127–130
12. G. Gertsberg, N. Nagar, M. Lautzker, B. Bronfin, N. Moscovitch, and S. Schumann, SAE paper 2005-01-0334, Detroit, MI, 2005